2004

In vivo dosimetry and seed localization in prostate brachytherapy with permanent implants

Anatoly B. Rosenfeld
University of Wollongong, anatoly@uow.edu.au

Dean Cutajar
University of Wollongong, deanc@uow.edu.au

M. L. Lerch
University of Wollongong, mlerch@uow.edu.au

G. J. Takacs
University of Wollongong, gjt@uow.edu.au

T. Braddock
University of Wollongong, braddock@uow.edu.au

See next page for additional authors

Publication Details

This article was originally published as: Rosenfeld, AB, Cutajar, DL, Lerch, MLF et al, In vivo dosimetry and seed localization in prostate brachytherapy with permanent implants, IEEE Transactions on Nuclear Science, December 2004, 51(6)1, 3013-3018.

In Vivo Dosimetry and Seed Localization in Prostate Brachytherapy With Permanent Implants

Anatoly B. Rosenfeld, *Senior Member, IEEE*, D. L. Cutajar, M. L. F. Lerch, *Member, IEEE*, G. J. Takacs, J. Brady, T. Braddock, V. L. Perevertaylo, *Member, IEEE*, J. Bucci, J. Kearsley, M. Zaider, and M. Zelefsky

***Abstract*—This paper reports on the development of an interactive, intraoperative dose planning system for seed implant brachytherapy in cancer treatment. This system involves *in vivo* dosimetry and the ability to determine implanted seed positions. The first stage of this project is the development of a urethral alarm probe to measure the dose along the urethra during a prostate brachytherapy treatment procedure. Ultimately, the system will be used to advise the physicians upon reaching a preset dose rate or dose after total seed decay in the urethra during the seed placement. The second stage is the development of a method and instrumentation for *in vivo* measurements of the location of implanted seeds in the same frame as for dose planning and the use of these in intraoperative treatment planning. We have developed a silicon mini-detector, miniature front-end, and shaping amplifier with discriminator, connected to the mini-silicon detector at the end of a cable placed in a urological catheter, to satisfy the spectroscopic requirements of the urethral probe. This technique will avoid complications related to overdosing the urethra and the rectum.**

I. Introduction

REAL-TIME transrectal ultrasound guided transperineal placement of permanent interstitial ^{125}I and ^{103}Pd sources is one of the treatment modalities available for early stage prostate cancer. There has been a rapid expansion of the use of this procedure, which is set to become the most common treatment modality for early stage prostate cancer. Equivalent biochemical control rates for low-risk prostate cancer with permanent seed implantation in comparison to radical prostatectomy or external beam radiotherapy have been confirmed [1], [2]. These biochemical outcomes have been favorable, but there has been little emphasis on the evaluation and comparison of side effects and complications. Interstitial brachytherapy exhibits a different side effect profile than radical prostatectomy or external beam radiotherapy. Specifically, acute urinary side effects predominate in interstitial prostate brachytherapy [3]–[5]. Urinary symptoms, resulting in an increase of the International Prostate Symptom Score (IPSS), are well-recognized side effects of interstitial prostate brachytherapy; however, more detailed evaluation of these symptoms has been lacking. Wallner *et al.* [6] observed an increase in grade-3 late urethral toxicity when the urethral dose exceeded 400 Gy. Recent recommendations by the American Brachytherapy Society (ABS) for reporting morbidity after prostate brachytherapy request urethral doses be recorded for correlation with urethral toxicity [7]. The ABS recommends that doses be obtained at the center of the urethra, in half-centimeter intervals, from the base to the apex of the prostate, reporting the maximum and mean obtained doses [7].

Medical complications associated with interstitial prostate brachytherapy can result from errors in seed placement during insertion. There are several factors that may lead to the misplacement of seeds. The guiding needles may diverge during insertion as different layers of tissue are penetrated [8], resulting in the incorrect deposition of seeds; the seeds may drift along the path of the needles; blood flow may alter the seed positions; oedema may alter the size and shape of the prostate; and gland motion may occur [9]. There is a need for seed locations to be monitored in real-time during insertion (intraoperatively). If a seed is misplaced, the required locations of other seeds may be recalculated in compensation. Intraoperative localization of inserted seeds will also provide a method of online dosimetry. Many difficulties have been encountered in the development of an interactive planning system in the operating theatre in prostate brachytherapy [10]. Current commercial systems use ultrasound visualization of individual seeds or needles to predict the dose within the prostate during treatment. These systems are expensive, have problems with artifacts as on two-dimensional ultrasound seed imaging and are unable to determine precisely the individual seed locations during a treatment procedure. The Memorial Sloan-Kettering Cancer Center (MSKCC) has developed an intraoperative conformal optimization and planning system (I-3D) for ultrasound-based transperineal prostate implants [11]. Optimal operation of this system requires accurate and reproducible real-time position coordinates of each successively implanted seed. The MSKCC has also recently developed an intraoperative dosimetry system for prostate brachytherapy based on the combination of two imaging techniques [12]. Ultrasound images are obtained of the prostate and lead markers, which are attached to the ultrasound probe. Fluoroscopic images of the implanted seeds and lead markers are also obtained. The seed locations obtained from the fluoroscopic images are superimposed onto the prostate images using computer reconstruction. The entire process takes approximately 10 min [12].

Brachytherapy seeds contain radioactive sources, usually ^{125}I or ^{103}Pd. These radioactive sources emit low-energy photons with a distinct energy spectrum, at very low-dose rates that are

Manuscript received November 15, 2003; revised April 17, 2004 and July 6, 2004.

A. B. Rosenfeld, D. L. Cutajar, M. L. F. Lerch, G. J. Takacs, J. Brady, and T. Braddock are with the Centre for Medical Radiation Physics, University of Wollongong, Wollongong, Australia.

V. L. Perevertaylo is with the SPO-BIT, Kiev, Ukraine.

J. Bucci and J. Kearsley are with the Institute for Prostate Cancer, St. George Cancer Care Centre, Kogerah, Australia.

M. Zaider and M. Zelefsky are with the Memorial Sloan-Kettering Cancer Center, New York, NY 10021 USA.

Digital Object Identifier 10.1109/TNS.2004.839089

TABLE I
6711 SEED PHOTON EMISSION [15]

Energy (keV)	Mean number/disintegration
35.492	0.0666
31.877	0.0438
30.980	0.201
27.472	0.756
27.202	0.405

hard to measure with conventional detectors in confined spaces. The complexity of the dosimetry of ^{125}I and ^{103}Pd seeds is due to the low-dose rates, anisotropy of dose about the seeds, and rapidly diminishing dose with distance from the seeds. Traditional *in vivo* dosimetry demands miniature, high sensitive and tissue equivalent dosimeters. Miniature on-line radiotherapy dosimeters currently available such as mosfets or diodes are energy dependent in this spectral range and are not sensitive enough.

Here, we propose the development of an alternative intraoperative dosimetry system based on *in vivo* spectroscopy. The spectroscopy method of dosimetry does not require tissue equivalency of the detector and is very sensitive. Spectroscopic dosimetry is based on separate photopeak analysis rather than the integral effect of all the photons as in the diode or mosfet dosimeter. Measurements of a particular low-energy X-ray photopeak of known energy can be used for dosimetry or distance measurements between a source and a detector. This can be achieved with a miniature X-ray Si detector operating in spectroscopy mode.

At low energies, approximately 27 keV for ^{125}I, most energy loss occurs through the photoelectric effect. The Compton scattering cross section is significant, but energy loss due to the Compton effect is minimal. In this case, the intensity of the photopeak at a distance r from the point source can be represented as $\mathrm{e}^{-\mu \mathrm{r}}/\mathrm{r}^2$, where μ is the attenuation coefficient for photons at a distinct energy penetrating a constant medium. Spectral peaks of different energies will be attenuated by different amounts as the emitted photons penetrate the tissue. Using the above principle, the ratio of peak heights or area under the peaks in an obtained spectrum will yield the distance from a point source to the detector. In the case of multiple seed implants (i.e., permanent seed implants) where each seed is implanted sequentially, the increase in the rate of change of area or peak height from one seed implant to the next will be used to deduce the newly implanted seed position. If the distance to one detector is known, the triangulation of distances from a noncoplanar array of detectors will yield the seed position. The ability of solid-state detectors to resolve the low-energy photons, such as those in Table I, is improving as new detector technologies are being developed. Such a system will be intraoperative and will allow online dosimetry of the treatment.

II. MATERIALS AND METHODS

Monte Carlo simulations and experimental measurements were performed on an OncoSeed number 6711 from Amersham Health [13]. This seed consists of radioactive ^{125}I, adsorbed onto a silver rod, encapsulated in a hollow titanium cylinder with welded ends. The geometry of the seed was obtained from Williamson [14]. The silver rod is 3 mm in length and 0.5 mm in diameter. A 1-μm-thick coating of silver halide is present on the rod. The radioactive iodine was assumed to be at the midpoint of the silver halide coating. The titanium shell was 4.5 mm in length, 0.8 mm in diameter, 0.06-mm thick along the sides, and 0.5-mm thick at the end welds. ^{125}I decays via electron capture, emitting photons of several distinct energies through gamma and X-ray emission. Internal conversion and Auger electrons are also emitted, but were neglected, as they would not penetrate the titanium shell. A 3.6-keV photon was also neglected.

Due to the presence of silver in the seed, silver fluorescent X-rays of energies 22.1 and 25.2 keV [16] are present.

Monte Carlo simulations were performed using EGSnrcV2 [17]. The FLURZnrc user code was used to simulate the 6711 seed in a liquid water phantom. The energy spectrum was obtained at various locations for distances up to 5 cm from the seed center at various angles around the seed. The real energy resolution of any detector used to measure these spectra was not taken into account during simulation. This resulted in the energy peaks being very sharp, occupying only one or two channels per peak in each energy spectrum. The area under each photon peak was calculated for each obtained spectrum. This equated to the total number of counts in the one or two channels occupied by each photopeak. The ratios of peak areas were calculated for the 27-, 31-, and 35-keV peak. These obtained peak ratios were plotted versus distance from the seed and angle about the seed axis. An algorithm relating peak ratio to seed location was then constructed.

Given that we have a method for determining the distance from a seed to a detector, and we have four or more noncoplanar detectors, we can determine the location of the seed. For example, if we have "n" detectors, each at a known location $\mathbf{r}_\mathrm{i}$, and the distance from each detector determined from analysis of the spectrum is $\mathrm{s_i}$, then we may determine the seed location from minimization of the following function:

$$\sum_{i=1}^{n} \left\{ (\mathbf{r} - \mathbf{r}_i) \bullet (\mathbf{r} - \mathbf{r}_i) - s_i^2 \right\}. \tag{1}$$

The location $\mathbf{r}$, which minimizes this, is then the estimate of the seed location.

III. RESULTS

From Fig. 1, it can be seen that the photon peaks in the energy spectrum of the 6711 seed are very sharp, with very little scattering, even after the photons have traversed 5 cm of liquid water. This allows the use of spectroscopy for analysis of the radiation throughout the prostate during interstitial brachytherapy. The areas under the 27-, 31-, and 35-keV peaks were calculated for each obtained spectra. Figs. 2 and 3 are plots of the ratio of the area under two separate peaks versus distance along the transverse axis of the seed.

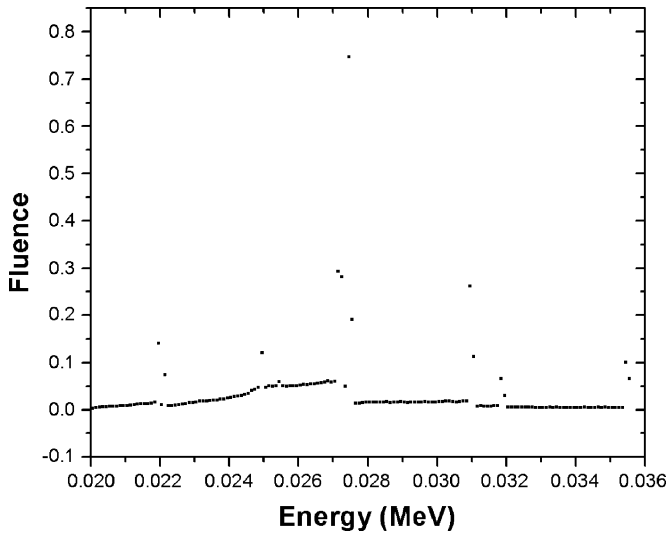

Fig. 1. FLURZnrc energy spectrum of a 6711 seed, measured 5 cm from seed along the transverse axis. After traversing 5 cm of water, the energy peaks are still very sharp, with minimal low-energy tails.

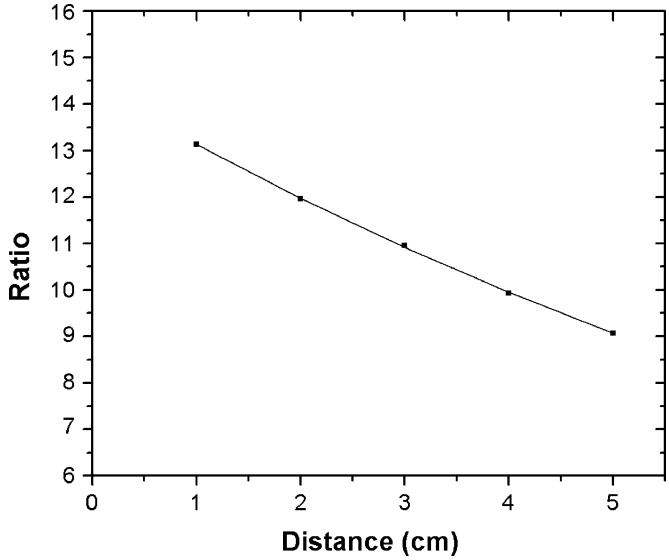

Fig. 2. Ratio of the area under the 27-keV peak to the area under the 35-keV peak versus distance along the transverse axis for the 6711 seed, obtained from the FLURZnrc spectra.

Since scattering is minimal and the majority of energy loss occurs through the photoelectric effect, the area under each peak as a function of distance may be given by

$$A = \frac{A_0 e^{-\mu r}}{r^2} \tag{2}$$

where A is the area under a single peak, A_0 is the area at zero distance, μ is the attenuation coefficient of the medium for photons of the peak energy, and r is the distance from the seed to the point of measurement. The ratio of the area under two peaks, a and b, may be given by

$$R^{\frac{a}{b}} = R_0^{\frac{a}{b}} e^{-\Delta\mu r} \tag{3}$$

where $R^{a/b}$ is the ratio of the area under peak a to the area under peak b, $R_0^{a/b}$ is the peak ratio at zero distance, and $\Delta\mu$ is the

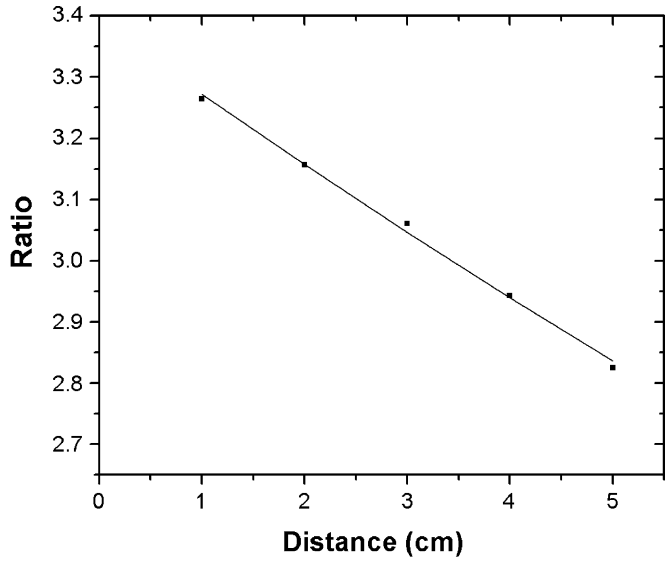

Fig. 3. Ratio of the area under the 31-keV peak to the area under the 35-keV peak versus distance along the transverse axis for the 6711 seed, obtained from the FLURZnrc spectra.

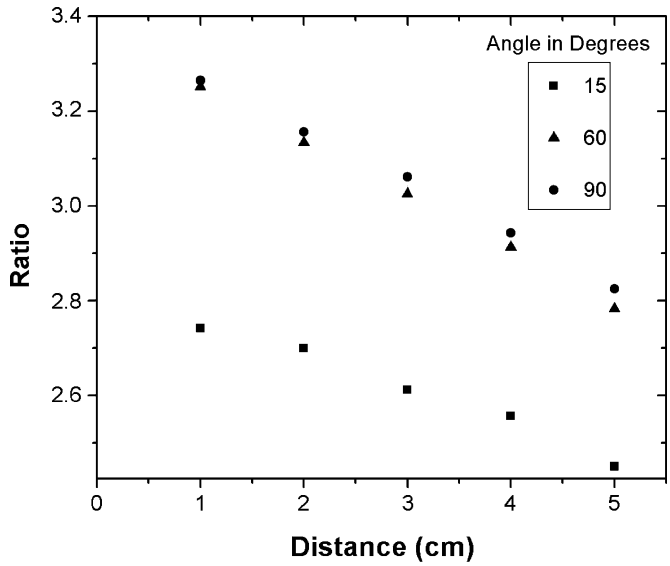

Fig. 4. Ratio of the area under the 27-keV peak to the area under the 35-keV peak versus distance for a 6711 seed in a water phantom, calculated at various angles around the seed. An angle of 90° represents measurements along the transverse axis of the seed.

difference in attenuation coefficients $(\mu_{\rm a} - \mu_{\rm b})$. Using (3) and the data obtained from the FLURZnrc simulations of the 6711 seed in water, the following equations were devised

$$R^{\frac{27}{35}} = 14.41e^{-0.093r} \pm 3\% \tag{4}$$

$$R^{\frac{31}{35}} = 3.39e^{-0.036r} \pm 4\%. \tag{5}$$

The distance to a 6711 seed within liquid water may be determined by calculating the ratio of the area underneath two peaks in the spectrum and using (4) or (5). This assumes the point of measurement is along the transverse axis of the seed.

The previous calculations were repeated for spectra obtained at different angles around a 6711 seed in a liquid water phantom. A plot of $R^{27/35}$ versus distance was obtained in Fig. 4.

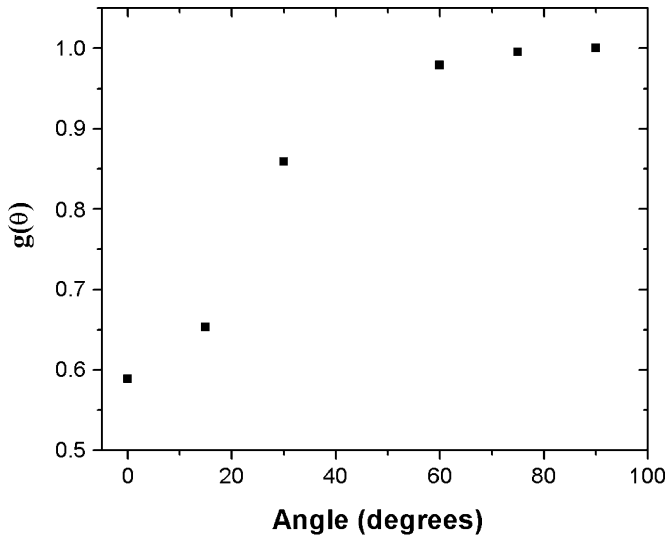

Fig. 5. Normalized plot of $\mathrm{R}^{27/35}$ versus the angle to determine the function $\mathrm{g}(\theta)^{27/35}$. Ratios were calculated 1 cm from the seed center for different angles.

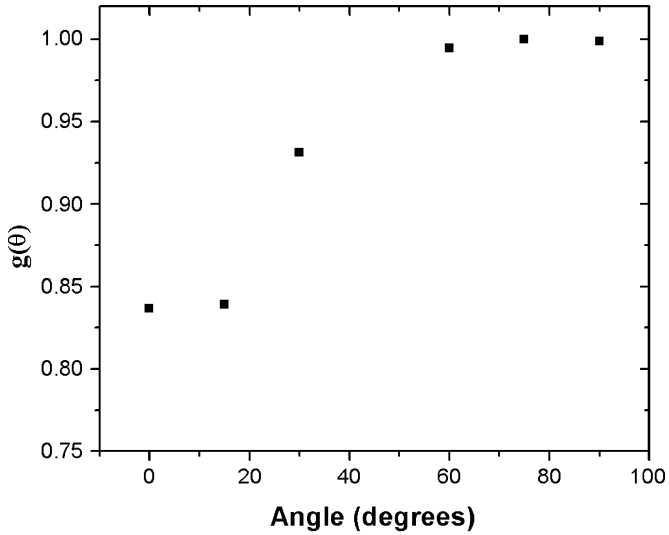

Fig. 6. Normalized plot of $\mathrm{R}^{31/35}$ versus the angle to determine the function $\mathrm{g}(\theta)^{31/35}$. Ratios were calculated 1 cm from the seed center for different angles.

It can be seen from Fig. 4 that the peak ratios vary with changes in source angle. This is due to the variation in thickness of the titanium shell around the seed. Photons at lower angles traverse a greater thickness of titanium, increasing the attenuation, lowering the peak ratios. Simply finding the ratio of any two peaks in a measured spectrum is not enough to determine the distance to the seed. The peak ratios are a function of both distance and angle. Assuming the distance from the seed to the detector is much larger than the thickness of the titanium jacket surrounding the source within the seed, the peak ratios may be represented as separable functions of both distance and angle

$$R = R_0 f(r) g(\theta) \tag{6}$$

where $f(r)$ is the distance dependent function of the peak ratio and $\mathrm{g}(\theta)$ is the angular dependent function of the peak ratio. $f(r)$ was previously found to be $e^{-\Delta\mu r}$. To determine the angular dependent function of the peak ratios $\mathrm{g}(\theta)$, the peak ratios versus angle were plotted for a distance of 1 cm, normalized, and shown in Figs. 5 and 6.

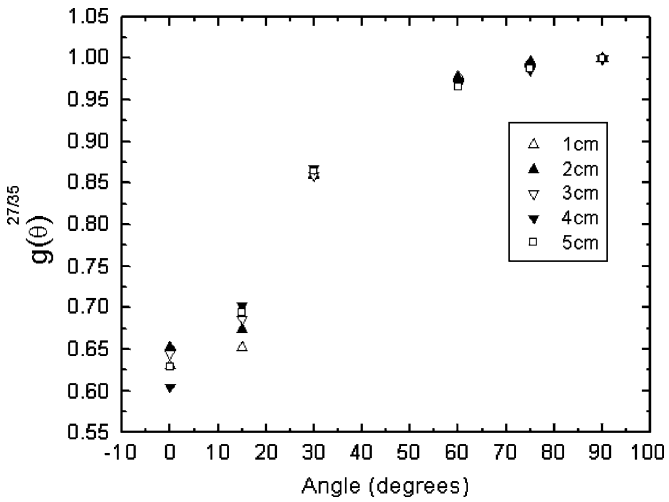

Fig. 7. Normalized plot of $\mathrm{R}^{27/35}$ versus the angle to determine the function $\mathrm{g}(\theta)^{27/35}$, for various distances from the seed center.

After taking into account the angular variance in peak ratios, (4) and (5) become

$$R^{\frac{27}{35}} = 14.41 e^{-0.093r} g(\theta)^{\frac{27}{35}} \pm 5\% \tag{7}$$

$$R^{\frac{31}{35}} = 3.39 e^{-0.036r} g(\theta)^{\frac{31}{35}} \pm 6\%. \tag{8}$$

By calculating the area under the 27-, 31-, and 35-keV peaks for an obtained spectrum, performing ratios of the obtained areas and solving (7) and (8) simultaneously, the distance to the seed as well as the angle of the seed to the point of measurement may be determined. Fig. 7 shows the normalized plot of $R^{27/35}$ versus angle for various distances up to 5 cm from the seed. The curves show a similar trend, with small discrepancies at low angles. These discrepancies are due to an increase in statistical error as the thicker titanium shell at the end welds of the seed greatly attenuates the photons, reducing the counts at low angles.

In order to determine the practicality of this approach for determining seed positions, we have conducted simulations where seeds are placed at random in a specified cubical treatment volume. The cubical volume has variable dimensions in order to see the effects of different prostate volumes on the feasibility of the method. Four detectors are placed in a tetrahedral configuration within the cubical treatment volume. The tetrahedral detector arrangement and the cubical treatment volume share a common center. A seed is placed at a randomly selected location in the treatment volume, as shown in Fig. 8.

The distance between each detector and the seed is calculated from the known coordinates. In practice, the distance that the seed is from a given detector will be determined by a signal from the detector. This will differ from the actual distance due to the effects of noise and uncertainties due to seed anisotropy. In order to simulate the effect of this uncertainty, each distance is varied randomly to introduce errors. These errors are uniform distributions in the range of $\pm 2\%$ and $\pm 5\%$. The uncertain distances s_i are then used, along with the known detector positions $\mathbf{ri}$, in (1). The seed location, r, which minimizes this expression, is then deduced using the downhill simplex method [18], and compared to the actual seed location. The distance between the deduced and actual seed location is recorded as the error for that seed location. This procedure is then repeated a large

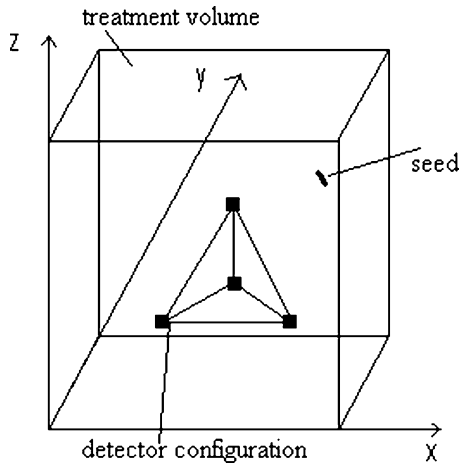

Fig. 8. Cubical treatment volume containing a centralized tetrahedral detector configuration and a brachytherapy seed at a randomly generated location within the treatment volume.

TABLE II
ERRORS IN SEED LOCATION

Cube edge length (cm)	Tetrahedron edge length (cm)	Error (%) in seed-detector distance	Average error (mm)	Percentage greater than 2.5mm
4.5	3.0	5	1.8	18
4.0	3.0	5	1.6	12
3.5	2.5	5	1.4	7
3.0	2.5	5	1.2	3
4.5	2.5	2	0.72	0.12
4.0	2.5	2	0.63	0.011
3.5	2.5	2	0.56	0.003
3.0	2.5	2	0.48	0.0012

number of times in order to get a reasonable idea of the range of errors for each configuration. The results of this process are summarized in Table II for various combinations of treatment volume size, tetrahedral detector configuration size, and for two different precisions in seed-detector distances.

The first column of Table II specifies the size of the cubical treatment volume. The tetrahedron dimensions are given in the second column. In the third column, we note the assumed uncertainty in the distance between the seed and detector. The average error, in the fourth column, refers to the average, over one million seed placements, of the difference in the seed position as returned by the function minimization and the known seed position. The final column lists the percentage of seeds for which an error of greater than 2.5 mm occurred.

The results of Table II show that the proportion of times a large seed location error occurs is sensitive to the precision with which the seed-detector distances can be determined. An increase in this error by a factor of 2.5 results in an increase by the same factor in the average error, but the proportion of times an error of greater than 2.5 mm occurs increases by a much greater factor. For a fixed experimental precision in determining seed-detector distances, the average error is proportional to the cube edge length of the treatment volume, or the treatment volume to the one-third power. Thus, if such a method should prove feasible, it should work better for smaller treatment volumes.

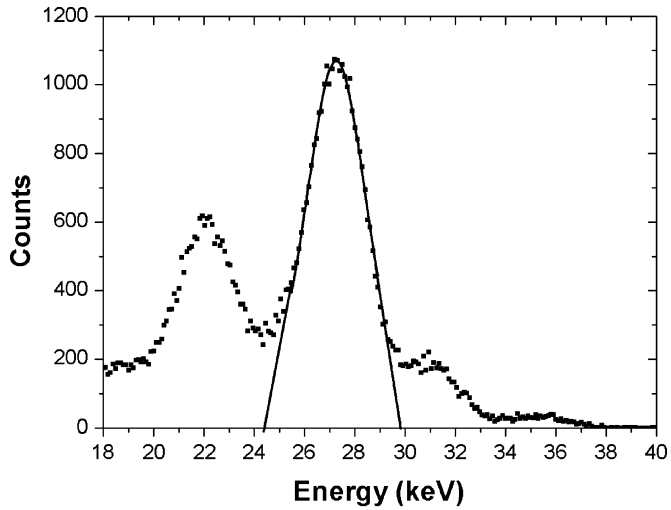

Fig. 9. The 6711 seed spectrum, measured with the urethra alarm probe connected to the preamplifier via a 40-cm cable. The 27-keV peak is well resolved. The 31 and 35-keV peaks are well resolved, but do not contain many counts. Also present is the 22-keV silver X-ray peak. The 27-keV peak is outlined and has a FWHM of 2.3 keV.

The described technique for seed localization measurements, in the case of permanent implants in a prostate, demands the placement of a minimum of four noncoplanar detectors. These mini-detectors will be placed in needles and will be introduced into the prostate prior to seed implantation. The detectors should be small enough to be inserted into a 1-mm diameter needle, and must be operated in spectroscopy mode with energy resolution suitable for the resolving of X-ray peaks from ^{125}I or ^{103}Pd seeds. An important issue is the efficiency of the detector, which should be enough to provide good statistics within a short time (1–3 s) after each seed has been implanted, while, on the other hand, pulse pile up should be avoided. When multiple seeds are present, each additional seed changes the rate of increase of counts in each channel. This increment in the count rate provides the spectral information, which is analyzed to determine the distance from each detector to the latest seed.

Currently, we have developed an *in vivo* dosimetry system for the urethra, the urethra alarm probe, as a first stage of the project. This uses spectroscopy to estimate the dose to the urethra during interstitial brachytherapy treatment. The probe consists of a silicon mini-detector of dimensions $0.8\times0.8\times3$ mm. This is connected to a preamplifier/amplifier system by a thin 40-cm cable, allowing the placement of the detector within the prostate via a urinary catheter. The described probe was used to measure the energy spectrum of a 6711 seed in air at 25 °C, while connected to the amplifier system via a 40-cm cable that would be used in practice. The resulting spectrum is shown in Fig. 9.

The 6711 seed spectrum in Fig. 9 demonstrates that the current detector system is able to resolve the peaks necessary for use in the seed localization procedure. Analysis of the ratio of the peak amplitudes measured in air does not correspond to the frequencies in Table I, as emitted by an ^{125}I source, or the ratios shown in Figs. 2 and 3. This is due to the efficiency of the silicon detector varying with incident photon energy. This efficiency needs to be taken into account in the proposed technique for seed location measurements. The photon spectrum of

the 6711 seed was also measured with the photons incident on the rear of the detector. There was no apparent change in the measured spectrum, indicating that the detector was fully depleted and has an isotropic response to photon irradiation.

IV. Conclusion

The the development of an intraoperative treatment planning system for low-dose rate brachytherapy of the prostate, based on *in vivo* spectroscopic dosimetry, has many advantages. The most important advantage is the allowance for seed localization, measured in real time. It was demonstrated that small Si detectors are a good choice for a spectroscopic localization system. Such a system will allow for updating of the treatment plan to correct for seed misplacement, and online dosimetry. A method exists for locating seeds, based on distances between each of four detectors and a seed, with each of these distances being determined by observation of the ratio of counts under different energy peaks. This method will need to be expanded for use in prostate brachytherapy where the seed count is large and seeds may be implanted too far from a detector to give an adequate response increment. To approach this, we propose the use of an array of at least 16 detectors, implanted on several needles. A data acquisition system will then be used to monitor the increment in counts from all detectors and choose the best combination of four noncoplanar detectors to be used for the localization algorithm. The determination of the distance from a seed to a detector is possible, theoretically, and is currently under investigation in a tissue equivalent phantom. The recently developed urethra alarm probe, based on a silicon mini-detector operating in spectroscopy mode, is the first stage of the project, and is suitable for real time dosimetry within the urethra, without the need for a tissue equivalent dosimeter.

References

[1] J. C. Blasko, P. D. Grimm, J. E. Sylvester, K. R. Badiozamani, D. Hoak, and W. Cavanagh, "Palladium-103 brachytherapy for prostate carcinoma," *Int. J. Radiat. Oncol., Biol., Phys.*, vol. 46, pp. 839–850, 2000.

[2] H. Ragde, A. A. Elgamal, P. B. Snow, J. Brandt, A. A. Bartolucci, B. S. Nadir, and L. J. Korb, "Ten-year disease free survival after transperineal sonography-guided iodine-125 brachytherapy with or without 45-gray external beam irradiation int the treatment of patients with clinically localized, low to high Gleason grade prostate carcinoma," *Cancer*, vol. 83, pp. 989–1001, 1998.

[3] D. Y. Gelblum, L. Potters, R. Ashley, R. Waldbaum, X. Wang, and S. Leibel, "Urinary morbidity following ultrasound-guided transperineal prostate seed implantation," *Int. J. Radiat. Oncol., Biol., Phys.*, vol. 45, pp. 59–67, 1999.

[4] N. Lee, C. Wuu, R. Brody, J. L. Laguna, A. E. Katz, E. Bagiella, and R. D. Ennis, "Factors predicting for postimplantation urinary retention after permanent prostate brachytherapy," *Int. J. Radiat. Oncol., Biol., Phys.*, vol. 48, pp. 1457–1460, 2000.

[5] G. S. Merrick, W. M. Butler, J. H. Lief, and A. T. Dorsey, "Temporal resolution of urinary morbidity following prostate brachytherapy," *Int. J. Radiat. Oncol., Biol., Phys.*, vol. 47, pp. 121–128, 2000.

[6] K. Wallner, J. Roy, and L. Harrison, "Dosimetry guidelines to minimize urethral and rectal morbidity following transperineal I-125 prostate brachytherapy," *Int. J. Radiat. Oncol., Biol., Phys.*, vol. 32, pp. 465–471, 1995.

[7] S. Nag, R. J. Ellis, G. S. Merrick, R. Bahnson, K. Walner, and R. Stock, "American Brachytherapy Society (ABS) recommendations for reporting morbidity after prostate brachytherapy," *Int. J. Radiat. Oncol., Biol., Phys.*, vol. 54, pp. 462–470, 2002.

[8] S. Nath, Z. Chen, N. Yue, S. Trumpore, and R. Peschel, "Dosimetric effects of needle divergence in prostate seed implant using 125-I and 103-Pd radioactive seeds," *Med. Phys.*, vol. 27, no. 5, pp. 1058–1066, 2000.

[9] R. Taschereau, J. Roy, and J. Pouliot, "Monte Carlo simulations of prostate implants to improve dosimetry and compare planning methods," *Med. Phys.*, vol. 26, no. 9, pp. 1952–1959, 1999.

[10] S. Nag, J. P. Ciezki, R. Cormack, S. Doggett, K. DeWyngaert, G. K. Edmundson, R. G. Stock, N. N. Stone, Y. Yu, and M. J. Zelefsky, "Intraoperative planning and evaluation of permanent prostate brachytherapy: report of the American brachytherapy," *Int. J. Radiat. Oncol., Biol., Phys.*, vol. 51, no. 5, pp. 1422–1430, Dec. 1, 2001.

[11] M. J. Zelefsky, Y. Yamada, G. Cohen, E. S. Venkatraman, A. Y. Fung, E. Furhang, D. Silvern, and M. Zaider, "Postimplantation dosimetric analysis of permanent transperineal prostate implantation: improved dose distributions with an intraoperative computer-optimized conformal planning technique," *Int. J. Radiat. Oncol., Biol., Phys.*, vol. 48, pp. 601–608, 2000.

[12] D. A. Todor, M. Zaider, G. N. Cohen, M. F. Worman, and M. J. Zelefsky, "Intraoperative dynamic dosimetry for prostate implants," *Phys. Med., Biol.*, vol. 48, pp. 1153–1171, 2003.

[13] Amersham Health, Inc., Princeton, NJ .

[14] J. F. Williamson, "Monte Carlo evaluation of specific dose constants in water for I-125 seeds," *Med. Phys.*, vol. 15, no. 5, pp. 686–694, 1988.

[15] E. Browne and R. B. Firestone, *Table of Radioactive Isotopes*, V. S. Shirley, Ed. New York: Wiley, 1986.

[16] C. Schell, C. C. Ling, Z. C. Gromadzki, and K. R. Working, "Dose distributions of model 6702 I-125 seeds in water," *Int. J. Radiat. Oncol. Biol. Phys.*, vol. 13, pp. 795–799.

[17] I. Kawrakow and D. W. O. Rogers, "The EGSnrc code system," NRC, Ottawa, ON, Canada, NRC Rep. PIRS-701, 2000.

[18] J. A. Nelder and R. Mead, *Comput. J.*, vol. 7, pp. 308–313, 1965.